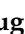





Article

Novel Sol-Gel Route to Prepare Eu^{3+} -Doped 80SiO_2 - 20NaGdF_4 Oxyfluoride Glass-Ceramic for Photonic Device Applications

María Eugenia Cruz ¹, Thi Ngoc Lam Tran ^{2,3,4}, Alessandro Chiasera ², Alicia Durán ¹, Joaquín Fernández ⁵, Rolindes Balda ^{6,7} and Yolanda Castro ^{1,*}

¹ Instituto de Cerámica y Vidrio, CSIC, 28049, Madrid, Spain

² IFN-CNR CSMFO Laboratory and FBK Photonics Unit, Via alla Cascata 56/C Povo, 38123 Trento, Italy

³ Department of Physics, Politecnico di Milano, Piazza Leonardo da Vinci 32, 20133 Milano, Italy

⁴ Department of Materials Technology, Faculty of Applied Science, Ho Chi Minh City University of Technology and Education, Vo Van Ngan Street 1, Thu Duc District, 720214 Ho Chi Minh City, Vietnam

⁵ Donostia International Physics Center (DIPC), 20018 San Sebastian, Spain

⁶ Department Física Aplicada, Escuela Superior de Ingeniería, Universidad del País Vasco (UPV-EHU), 48013 Bilbao, Spain

⁷ Centro de Física de Materiales, (CSIC-UPV/EHU), 20018 San Sebastian, Spain

* Correspondence: castro@icv.csic.es

Abstract: Oxyfluoride glass-ceramics (OxGCs) with the molar composition 80SiO_2 - $20(1.5\text{Eu}^{3+}:\text{NaGdF}_4)$ were prepared with sol-gel following the “pre-crystallised nanoparticles route” with promising optical results. The preparation of 1.5 mol % Eu^{3+} -doped NaGdF_4 nanoparticles, named $1.5\text{Eu}^{3+}:\text{NaGdF}_4$, was optimised and characterised using XRD, FTIR and HRTEM. The structural characterisation of 80SiO_2 - $20(1.5\text{Eu}^{3+}:\text{NaGdF}_4)$ OxGCs prepared from these nanoparticles’ suspension was performed by XRD and FTIR revealing the presence of hexagonal and orthorhombic NaGdF_4 crystalline phases. The optical properties of both nanoparticles’ phases and the related OxGCs were studied by measuring the emission and excitation spectra together with the lifetimes of the $^5\text{D}_0$ state. The emission spectra obtained by exciting the Eu^{3+} - O^{2-} charge transfer band showed similar features in both cases corresponding the higher emission intensity to the $^5\text{D}_0 \rightarrow ^7\text{F}_2$ transition that indicates a non-centrosymmetric site for Eu^{3+} ions. Moreover, time-resolved fluorescence line-narrowed emission spectra were performed at a low temperature in OxGCs to obtain information about the site symmetry of Eu^{3+} in this matrix. The results show that this processing method is promising for preparing transparent OxGCs coatings for photonic applications.

Keywords: oxyfluoride glass-ceramics OxGCs; sol-gel pre-crystallised nanoparticles route; NaGdF_4



Citation: Cruz, M.E.; Ngoc Lam Tran, T.; Chiasera, A.; Durán, A.; Fernández, J.; Balda, R.; Castro, Y. Novel Sol-Gel Route to Prepare Eu^{3+} -Doped 80SiO_2 - 20NaGdF_4 Oxyfluoride Glass-Ceramic for Photonic Device Applications. *Nanomaterials* **2023**, *13*, 940. <https://doi.org/10.3390/nano13050940>

Academic Editors: Antonios Kelarakis and Jean-Marie Nedelec

Received: 31 January 2023

Revised: 1 March 2023

Accepted: 3 March 2023

Published: 5 March 2023



Copyright: © 2023 by the authors. Licensee MDPI, Basel, Switzerland. This article is an open access article distributed under the terms and conditions of the Creative Commons Attribution (CC BY) license (<https://creativecommons.org/licenses/by/4.0/>).

1. Introduction

The development of transparent glass-ceramics (GC) has drawn the attention of numerous researchers, and they have been extensively studied due to their important optical applications [1]. GCs can be used for light-emitting diodes, solar cells, sensing catalysis or in biomedical materials [2,3]. Particularly, when fluoride nanocrystals smaller than 40 nm are dispersed in an oxide glass matrix, the resulting materials are transparent GCs, called oxyfluoride glass-ceramics (OxGCs), which have attractive properties [4]. These materials are transparent from the visible to near-infrared region and are compatible with new optical devices for communications or sensors. Furthermore, OxGCs retain the most relevant properties of glasses—good mechanical and thermal stability—and present properties characteristic of fluoride crystals as an effective optical media for light propagation and luminescence enhancement, and a high linear and nonlinear refractive index [5–8]. The crystal structure of fluorides as hosts of RE ions reduces the probabilities of multiphonon relaxation, resulting in high luminescence efficiencies [9–12]. Thus, the efficiency of the emission, optical transmission and spectra profile can be modified depending on the fluoride phase

and the dopant. Among fluoride nanoparticles, those with the formula $ALnF_4$ (where A is an alkaline element and Ln a lanthanide) have become more attractive in comparison to other fluorides due to their lowest phonon energies and wide band gap (9–10 eV) [13]. Particularly, $NaGdF_4$ nanoparticles have been prepared both in cubic (α -phase) and hexagonal (β -phase). Thoma, B.R.E. et al. [14] reported the influence of a precursors ratio to prepare either a cubic or hexagonal phase, and later, You, F. et al. [15] presented the lattice parameters of both phases and studied the optical behaviour of the Eu^{3+} -doped nanoparticles with promising results. In the last decade, many authors reported the preparation of RE-doped $NaGdF_4$ nanoparticles and their luminescent properties, showing their excellent behaviour for both down and up conversion processes [16–18]. Oxyfluoride glass-ceramics with $NaGdF_4$ have also been prepared using a melting-quenching process (MQ) [19]. The preparation of GCs via MQ requires the melting of inorganic raw materials at high temperatures (1400 °C–1700 °C) followed by a controlled heat treatment for generating precipitation and crystal growth. In 2013, Herrmann, A. et al. [20] obtained the $NaGdF_4$ in cubic and **hexagonal** phases by heat treatment at 750 °C. One of the limitations of the MQ process is the low maximum amount of active phase that can be obtained due to the volatilisation of fluorides at the high temperatures needed in the process. In addition, in many cases, MQ materials require very long heat treatments (3 h–80 h) to reach the desired crystallisation. Moreover, OxGCs prepared by MQ are usually bulk materials, and this processing method is not suitable for preparing coatings [20–23].

Sol-gel (SG) appeared as an alternative method, emphasised in the chemistry of the process, to avoid the drawbacks of MQ [24–26]. It is a favourable process through which highly homogeneous materials can be obtained at low temperatures (<500 °C) [27,28]. Furthermore, various material forms, e.g., bulks, powders and coatings, can be processed through the hydrolysis and polycondensation of metal alkoxide precursors, such as tetraethyl orthosilicate (TEOS) in a solvent, typically alcohol. Sol-gel allows us to control the structures in the molecular scale of the materials throughout the whole process, allowing for the preparation of highly homogeneous materials [29].

In 2019, Velázquez, J.J. et al. [13] reported the preparation of novel transparent OxGCs with $NaGdF_4$ using the sol-gel technique. The authors reported the precipitation of β - $NaGdF_4$ crystals through the heat treatment of a sol prepared in two steps, commonly called the TFA route [30]. In this case, silica precursors are mixed with a solution of rare-earth precursors in TFA, followed by a controlled heat treatment. The optical results obtained showed an efficient energy transfer from Gd^{3+} to Eu^{3+} as well as comparable lifetime values compared with the literature. Nevertheless, the OxGCs materials prepared using the TFA route are limited to transparent self-supported layers and powders. Although transparent and homogeneous OxGCs coatings were prepared using the TFA route, the densification of the films occurred during the heat treatment and concurrently with the crystallisation process, resulting in crystals that were too small, with sizes below 3 nm. The emission spectra of these OxGCs coatings revealed that rare-earth ions were located in an amorphous environment, suggesting that they were not successfully incorporated into the crystals, probably due to their small size [31].

In 2020, the GlaSS group from the Instituto de Cerámica y Vidrio (CSIC) reported an alternative route, labelled as the “pre-crystallised nanoparticles route” [30], based on the previous synthesis of crystalline fluoride nanoparticle aqueous suspensions that are subsequently incorporated into a silica sol [32]. Using this method, it is possible to control the morphology and size of the nanocrystals before their incorporation into the silica matrix. In a previous work, Cruz et al. [32] reported the preparation of Nd^{3+} -doped $80SiO_2$ - $20LaF_3$ oxyfluoride glass-ceramic powders via the pre-crystallised nanoparticles route with encouraging photonic results. The authors studied the stability of the LaF_3 nanoparticles in the silica matrix before and after the heat treatment at 450 °C, reporting the best luminescence results after the heat treatment when organics are eliminated. The optical characterisation of the OxGCs powders was also reported, with similar lifetimes to those for nanoparticles. Later, the GlaSS group reported the preparation of OxGCs coatings

with the composition Nd^{3+} -doped 80SiO_2 - 20LaF_3 , obtaining a bulk-like lifetime value of $440 \mu\text{s}$ [33].

A key point of the “pre-crystallised nanoparticles route” is the processing of the fluoride nanoparticle suspensions. Some authors reported the preparation of NaGdF_4 nanoparticle suspensions [34–37]. In 2004, Mech et al. [38] stated for the first time the preparation via hydrothermal synthesis of Eu^{3+} -doped NaGdF_4 and KGdF_4 nanoparticles [38,39]. They prepared the nanoparticles by mixing the rare-earth oxides in a hydrochloric acid solution with further incorporation of sodium fluoride. The results were auspicious, showing good optical properties, with sharp and well-defined peaks for Eu^{3+} emissions through the excitation of Gd^{3+} . Later, Sudheendra, L. et al. [40] described the preparation of Eu^{3+} -doped NaGdF_4 using a sodium citrate solution, indicating that the Gd^{3+} - Eu^{3+} host–dopant couple is the best system for down-conversion after UV excitation as the emission energy transition within Gd^{3+} can resonantly couple to the excited state of Eu^{3+} ions. The authors demonstrated that in Eu^{3+} -doped NaGdF_4 nanoparticles, the emission of the hexagonal phase is 25% more intense than those of the cubic structure. Although different papers reported the preparation of powdered NaGdF_4 nanoparticles via hydrothermal synthesis in an autoclave controlling the pressure and temperature [40–42], only a few papers have reported the use of this process to obtain aqueous nanoparticle suspensions to control the morphology of the nanoparticles.

The objective of this work was the preparation and characterisation of optically active oxyfluoride glass-ceramics through the incorporation of Eu^{3+} -doped NaGdF_4 nanoparticle aqueous suspensions into a silica sol. In this work, powdered glass-ceramics were prepared, and the suitability of this processing method to prepare transparent OxGCs was demonstrated. This is a promising method for preparing transparent coatings and overcoming the drawbacks of the traditional melting-quenching method. Moreover, the selection of Eu^{3+} ions as a dopant is due to its excellent properties as a local probe, providing important information on the environmental structure where it is located [43].

2. Materials and Methods

2.1. Synthesis of 1.5Eu^{3+} : NaGdF_4 Aqueous Suspensions

Nanoparticle suspensions of NaGdF_4 undoped and doped with 1.5 mol. % Eu^{3+} were prepared by mixing gadolinium nitrate ($\text{Gd}(\text{NO}_3)_3$, Merk) with europium acetate ($\text{Eu}(\text{CH}_3\text{CO}_2)_3$, Merk) in a molar ratio of $1\text{Gd}(\text{NO}_3)_3$: $0.015\text{Eu}(\text{CH}_3\text{CO}_2)_3$ with 20 mL of water at room temperature to obtain a homogeneous solution. After 30 min of stirring, 1 g of sodium fluoride (NaF , Merk) was incorporated into the solution, before stirring for another 15 min at room temperature. The final solution was transferred to a Teflon cup and put into a stainless-steel autoclave, heated up to 180°C and maintained for 20 h and 24 h. The suspensions were collected and used directly. The nanoparticles were labelled according to the reaction time: 1.5Eu^{3+} : NaGdF_4 -20 or 1.5Eu^{3+} : NaGdF_4 -24.

2.2. Synthesis of OxGCs with Composition 80SiO_2 - $20(1.5\text{Eu}^{3+}$: $\text{NaGdF}_4)$

OxGCs with the composition 80SiO_2 - $20(1.5\text{Eu}^{3+}$: $\text{NaGdF}_4)$ were prepared following the “pre-crystallised nanoparticles route” [30]. First, tetraethyl orthosilicate (TEOS, Sigma Aldrich) and methyl-triethoxysilane (MTES, ABCR) were mixed with a molar ratio of 1TEOS:1MTES, followed by the incorporation of the previously prepared aqueous nanoparticle suspensions, 1.5Eu^{3+} : NaGdF_4 -24, to reach a final molar relation of 80SiO_2 - $20(1.5\text{Eu}^{3+}$: $\text{NaGdF}_4)$. After the incorporation of the nanoparticle suspensions, concentrated hydrochloric acid (HCl, Sigma Aldrich) was added under vigorous stirring to catalyse the hydrolysis and condensation reactions. The solution was immersed in an ice bath for 2 min to stop the reaction. After that, the sol was stirred for 15 min at room temperature. Finally, absolute ethanol was used to dilute the final sol up to a final concentration of 171 g L^{-1} .

2.3. Characterisation of 1.5Eu³⁺: NaGdF₄ Aqueous Suspensions

1.5Eu³⁺: NaGdF₄-20 and 1.5Eu³⁺: NaGdF₄-24 suspensions were centrifuged at 6000 rpm for 5 min, and the resulting powders were rinsed with deionised water; the rinsing process was repeated three times. The powders were dried at 75 °C overnight, then heat-treated at 450 °C and 550 °C for 5 h in an oven in an air atmosphere and further characterised.

X-ray diffractions were used to characterise the powders of both compositions Eu³⁺: NaGdF₄-20 heat-treated at 450 °C for 5 h and Eu³⁺: NaGdF₄-24 heat-treated at 450 °C and 550 °C for 5 h using an X-ray powder diffractometer (D8 advance, Bruker) with CuK_α radiation (λ = 1.5406 Å). The diffraction patterns were acquired in the range 10° < 2θ < 70° with a step of 0.03°. The nano-crystalline sizes were calculated by using the Scherrer equation shown in Equation (1).

$$D_{hkl} = \frac{k\lambda}{\sqrt{\beta^2 - b^2 - \cos \theta}} \quad (1)$$

where D_{hkl} is the calculated crystallite size, $k = 0.94$ for spherical crystals, θ is the Bragg angle, β is the full width of the diffraction peak at half maximum intensity (FWHM) and b is the correction of the instrument. The fits were performed using Origin software and the pseudo-Voigt function.

The size was also calculated using the Williamson–Hall (W-H) plot from which the strain broadening was estimated. To perform the W-H plot, the peak width was studied as a function of 2θ degree. The strain (\mathcal{E}) was calculated using Equation (2) for each peak of the XRD pattern. By using the calculated \mathcal{E} and the D_{hkl} taken from the Scherrer equation (Equation (1)) for all peaks, a linear regression was generated with its corresponding slope and y-intercept. Considering that the linear regression corresponds to Equation (3), the strain component was calculated from the slope and the crystallite size from the y-intercept [33,34,44].

$$\mathcal{E} = \frac{\beta}{4\cos \theta} \quad (2)$$

$$\beta \cos \theta = K\lambda \frac{1}{D_{hkl}} + 4\mathcal{E} \sin \theta \quad (3)$$

Fourier transform infrared spectroscopy (FTIR) spectra of undoped NaGdF₄ NPs, 1.5Eu³⁺: NaGdF₄-24 dried at 75 °C overnight and 1.5Eu³⁺: NaGdF₄-24 heat-treated at 450 °C for 5 h were recorded using Perkin–Elmer spectrum 100 FT-IR equipment, in the range of 4000 cm⁻¹–450 cm⁻¹ with a resolution of 4 cm⁻¹.

High-Resolution Transmission Electron Microscopy (HRTEM) was used to characterise 1.5Eu³⁺: NaGdF₄ NPs heat-treated at 450 °C for 5 h. The powder was re-dispersed in ethanol and then dripped onto a carbon-coated copper grid (Lacey Carbon, LC-200-Cu 25/pk). HRTEM images were taken with a HRTEM-JEO 2100 microscope, and the particle size distribution was determined through ImageJ[®] software, using a maximum of 10 images. The lattice parameters of NaGdF₄ were determined using the Image-J source.

2.4. Characterisation of OxGCs with Composition 80SiO₂-20(1.5Eu³⁺: NaGdF₄)

The OxGCs with the composition 80SiO₂-20(1.5Eu³⁺: NaGdF₄) was dried at 75 °C overnight and then heat-treated at 450 °C for 5 h.

Structural properties of OxGCs powders were studied using X-ray diffraction (XRD) following the procedure described in Section 2.3. In addition, FTIR spectra of 80SiO₂-20(1.5Eu³⁺: NaGdF₄) OxGCs before and after the heat treatment were also performed following the setup described in Section 2.3.

2.5. Optical Characterisation

Room temperature emission and excitation spectra, as well as luminescence decays of 1.5Eu³⁺: NaGdF₄ NPs and OxGCs with the composition 80SiO₂-20(1.5Eu³⁺: NaGdF₄), with

both powders heat-treated at 450 °C for 5 h, were recorded by using a FS5 fluorescence spectrometer (Edinburg Instruments Ltd., UK) equipped with a 150 W xenon lamp. The lifetime value estimation was performed by fitting the exponential decay. The emission was detected using a Hamamatsu R928P photomultiplier.

The absolute photoluminescence quantum yield (PL QY) measurements were studied by using Hamamatsu Quantaaurus-QY C11347-11, utilising an integrated sphere to measure all luminous flux. The excitation source was a 150 W xenon light source. The absolute photoluminescence quantum yield was measured under excitation wavelength $\lambda_{exc} = 270 \pm 10$ nm, and the considered PL range for the QY calculation was from 400 nm to 700 nm. The procedure of each measurement was as follows: (i) measurement of a quartz Petri dish with cap, (ii) measurement of the quartz Petri disk containing the powder with cap, and (iii) calculation of the PL QY, following Equation (4).

$$\text{PL QY} = \frac{\text{Number of photons emitted as PL from the sample}}{\text{Number of photons absorbed by the sample}} \quad (4)$$

This measurement was repeated 10 times, and the final value of absolute photoluminescence quantum yield was obtained as the average of the 10 measurements.

Resonant time-resolved fluorescence line-narrowed (TRFLN) spectra of the ${}^5\text{D}_0 \rightarrow {}^7\text{F}_{0,1,2}$ transitions of Eu^{3+} were performed by exciting the OxGCs with the composition $80\text{SiO}_2\text{-}20(1.5\text{Eu}^{3+}:\text{NaGdF}_4)$ heat-treated at 450 °C for 5 h into the ${}^7\text{F}_0 \rightarrow {}^5\text{D}_0$ transition with a pulsed frequency doubled Nd: YAG pumped tuneable dye laser of 9 ns pulsed width and 0.08 cm^{-1} linewidth and detected by an EGG&PAR Optical Multichannel Analyzer. The measurements were carried out by keeping the sample temperature at 9 K in a closed cycle helium cryostat.

3. Results and Discussion

3.1. Structural Characterisation of $1.5\text{Eu}^{3+}:\text{NaGdF}_4$ NPs

Stable aqueous suspensions of NaGdF_4 nanoparticles, undoped and doped with 1.5Eu^{3+} , were successfully prepared at two reaction times (20 h and 24 h). Then, $1.5\text{Eu}^{3+}:\text{NaGdF}_4\text{-}20$ and $1.5\text{Eu}^{3+}:\text{NaGdF}_4\text{-}24$ nanoparticle suspensions were centrifuged and dried at 75 °C overnight to obtain the powders. Both powders were heat-treated at 450 °C for 5 h and characterised by X-ray diffraction in the range $10^\circ < 2\theta < 70^\circ$. The XRD diffractograms, shown in Figure 1a, confirm the crystallisation of NaGdF_4 in the hexagonal phase (JCPDS 28-1085) as the only appearing phase. Nevertheless, the definition of the peaks increases when increasing the reaction time from 20 to 24 h, suggesting bigger and better crystallised nanoparticles. The differences observed in the intensities of the peaks of XRD patterns are associated with a preferential orientation of the nanoparticles. This phenomenon can occur mainly due to the method of preparing the XRD samples. In the present work, the XRD samples were prepared by pressing the powder on a glass substrate with a small amount of Vaseline. Thus, the pressing procedure on the glass substrate could generate the preferential orientation of the nanoparticles. However, this procedure was chosen because the preparation of samples using other routes, such as putting the powder directly on the sample holder, could lead to the contamination of the XRD equipment [45].

The particle size, calculated using the Scherrer equation, increased from 30 nm to 70 nm for a reaction time of 20 to 24 h, respectively. He, F. et al. [46] described the preparation of hexagonal NaGdF_4 nanoparticles via hydrothermal synthesis where the crystal size increased from 170 nm to 1 μm when the reaction time increased from 2 h to 24 h. The growth of NaGdF_4 nanoparticles during hydrothermal synthesis is associated with a nucleation process followed by a crystal growth. Thus, the nucleation rate determines the growing crystal rate, and both processes are in competition [47].

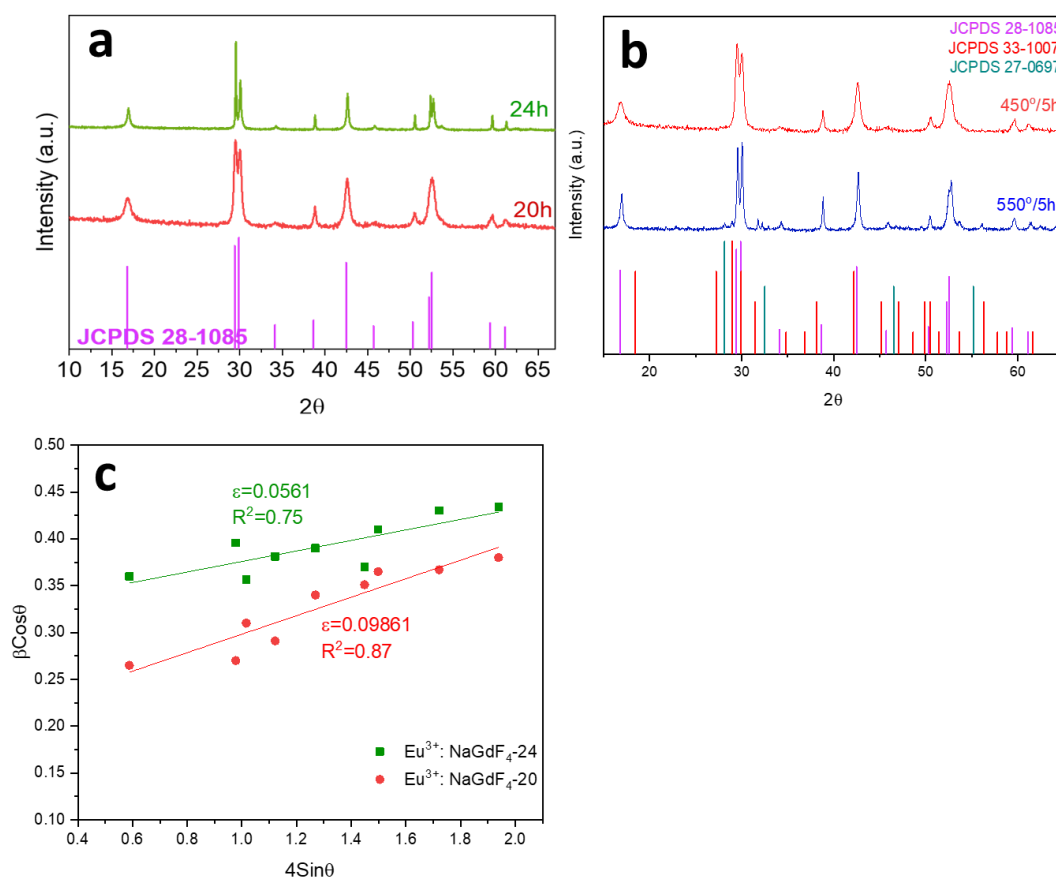


Figure 1. XRD patterns of (a) 1.5Eu^{3+} : NaGdF_4 NPs synthesised for 20 h and 24 h at $180\text{ }^\circ\text{C}$ in the autoclave; (b) 1.5Eu^{3+} : NaGdF_4 NPs synthesised for 20 h at $180\text{ }^\circ\text{C}$ and heat-treated at $450\text{ }^\circ\text{C}$ and $550\text{ }^\circ\text{C}$ for 5 h. (c) Williamson–Hall plot from the XRD of 1.5Eu^{3+} : NaGdF_4 NPs synthesised for 20 h and 24 h.

To avoid a scattering process associated with large nanoparticle size or their agglomerations, a reaction time of 20 h was selected for the rest of the studies, to ensure particle sizes below 30 nm.

Furthermore, 1.5Eu^{3+} : NaGdF_4 -20 nanoparticle suspension was sintered and heat-treated at $450\text{ }^\circ\text{C}$ or $550\text{ }^\circ\text{C}$ for 5 h. Figure 1b shows the XRD pattern of 1.5Eu^{3+} : NaGdF_4 -20 NPs heat-treated at $450\text{ }^\circ\text{C}$ and $550\text{ }^\circ\text{C}$ for 5 h. In the case of 1.5Eu^{3+} : NaGdF_4 -20 nanoparticles heat-treated at $550\text{ }^\circ\text{C}$, a partial transformation of hexagonal to cubic (JCPDS 27-0697) and orthorhombic (JCPDS 33-1007) phases is observed, associated with the presence of peaks at $2\theta = 31^\circ$ and 56° , while only the hexagonal phase is detected at $450\text{ }^\circ\text{C}$. For this reason, a sintering condition of $450\text{ }^\circ\text{C}$ for 5 h was chosen to ensure the presence of the hexagonal phase as unique.

Figure 1c shows the W-H plot corresponding to the 1.5Eu^{3+} : NaGdF_4 -20 and 1.5Eu^{3+} : NaGdF_4 -24, both heat-treated at $450\text{ }^\circ\text{C}$ for 5 h. The strain of the crystallites was calculated from the slope of each linear regression, and the strain decreases from 0.0986 to 0.0561 for 1.5Eu^{3+} : NaGdF_4 -20 to 1.5Eu^{3+} : NaGdF_4 -24, respectively. Moreover, the particle size, calculated from the y-intercept, increases from 16 nm for the sample 1.5Eu^{3+} : NaGdF_4 -20 to 60 nm for 1.5Eu^{3+} : NaGdF_4 -24. The fact that the crystal size calculated using the W-H plot for Eu^{3+} : NaGdF_4 -20 is around half that calculated using the Scherrer equation likely indicates that a great part of the width of the XRD peaks corresponds to the intrinsic strain of the nanoparticles. By contrast, nanoparticles obtained with a high reaction time (1.5Eu^{3+} : NaGdF_4 -24) present lower differences between the crystallite size calculated using the W-H and Scherrer equations, evidencing smaller strain contributions, probably due to nanoparticles with a bigger size and higher molecular order.

Figure 2 shows the HR-TEM images corresponding to $1.5\text{Eu}^{3+}:\text{NaGdF}_4$ -20 nanoparticles heat-treated at $450\text{ }^\circ\text{C}$ for 5 h. Figure 2a shows nanoparticles with irregular shapes and sizes around 30 nm, around double of that calculated with the W-H plot, which is associated with the tendency of nanoparticles to agglomerate during synthesis and further centrifugation to obtain powders. The hexagonal shape is not clearly observed, probably due to the low amount of phase present in the nanoparticles. Wu, Y. et al. [48] reported the hydrothermal preparation of hexagonal NaGdF_4 NPs using the same temperature and reaction times, observing that when NaF is used as a fluoride precursor, and for $\text{pH} = 7$, nanoparticles tend to have irregular shapes, as shown in this work. The size distribution is shown in Figure 2b, and a broad peak is observed with NP sizes between 20 nm and 42 nm with an average size of 34 nm. Figure 2c shows an amplified image of Figure 2a, revealing the existence of pores of around 2.5–3 nm inside the NP. The presence of pores can be attributed to a rapid formation of the nanoparticles followed by a long time for growing during which pores can be formed, as mentioned before [49]. The corresponding fast Fourier transform (FFT) pattern from the marked area in Figure 2d displays an interplanar distance of nearly 0.36 nm associated with the (001) plane of the NaGdF_4 hexagonal phase, confirming the XRD results.

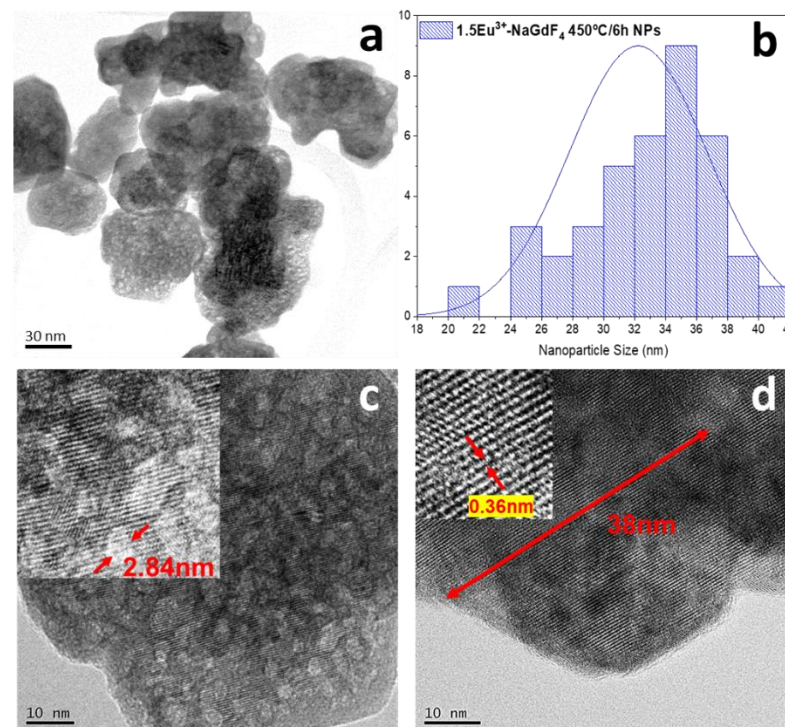


Figure 2. HR TEM images of (a) $1.5\text{Eu}^{3+}:\text{NaGdF}_4$ NPs heat-treated at $450\text{ }^\circ\text{C}$ for 5 h; (b) the corresponding nanoparticle size distribution taken from the image on “a”; (c) amplification of the area selected in “a” with the porous size measurement; (d) amplification of the area selected in “a” with the lattice distance measurement.

The structural characterisation of the $1.5\text{Eu}^{3+}:\text{NaGdF}_4$ nanoparticles reveals that, even though $1.5\text{Eu}^{3+}:\text{NaGdF}_4$ -24 nanoparticles show a higher crystallisation degree, those synthesised for 20 h are more suitable for being incorporated into silica sol due to their smaller particle size. Moreover, a heat treatment of $450\text{ }^\circ\text{C}$ for 5 h was chosen for these nanoparticles to avoid undesired crystallisation together with the hexagonal NaGdF_4 . For these reasons, 20 h was selected as the best reaction time to prepare NaGdF_4 nanoparticle suspensions to carry out the further preparation of the OxGCs, and a heat treatment of $450\text{ }^\circ\text{C}$ for 5 h as the best condition for sintering and performing the further characterisations.

3.2. Structural Characterisation of 80SiO₂-20(1.5Eu³⁺: NaGdF₄) OxGCs Powders

OxGCs with the composition 80SiO₂-20(1.5Eu³⁺: NaGdF₄) were prepared through the incorporation of 1.5Eu³⁺: NaGdF₄-20 nanoparticles in aqueous suspension in the silica sol precursors. For XRD characterisation, the 80SiO₂-20(1.5Eu³⁺: NaGdF₄) sol was dried and heat-treated at 450 °C for 5 h. Figure 3 shows the presence of hexagonal (JCPDS 28-1085) and orthorhombic (JCPDS 33-1007) phases. The partial phase transformation can be attributed to the change in pH during the preparation of the sol, from pH 7 of NP suspension to pH 2 of the final sol. Some authors reported that the nanoparticles with the formula NaLnF₄ (Ln = Gd, Y, Li) are very sensitive to pH changes [46,50].

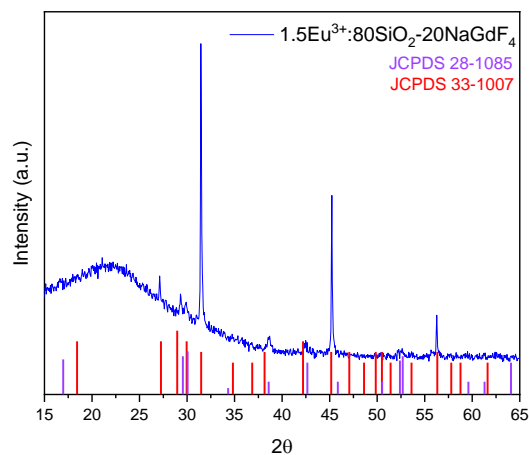


Figure 3. XRD pattern of OxGCs with the composition 80SiO₂-20(1.5Eu³⁺: NaGdF₄) heat-treated at 450 °C for 5 h.

Figure 4a shows the FTIR spectra obtained for undoped and 1.5Eu³⁺-doped NaGdF₄ nanoparticles heat-treated at 450 °C for 5 h (violet and blue line, respectively) and 80SiO₂-20(1.5Eu³⁺: NaGdF₄) heat-treated at 450 °C for 5 h and dried at 75 °C overnight (red and green line, respectively) in the range of 4000 cm⁻¹ to 400 cm⁻¹. In all cases, no clear peaks were detected in the range of 3000 cm⁻¹–4000 cm⁻¹, indicating that the materials were free of water (-OH bonds should appear around 3000–3500 cm⁻¹). Figure 4b shows the amplified spectra between 1500 cm⁻¹ and 400 cm⁻¹. In the 1.5Eu³⁺-doped NaGdF₄ nanoparticles, at around 500 cm⁻¹, a rising peak is identified associated with the tetrafluoride bond vibration [51] and confirming the formation of NaGdF₄ nanoparticles. This peak is not completely observed due to the range limitation of the equipment. A small peak at 807 cm⁻¹ and a broad double peak around 1114 cm⁻¹ are also observed, associated with traces of Gd-O bonds, indicating the presence of oxygen defects in the nanoparticle lattice [52,53]. These defects could be due to the reactions of acetates with nitrate precursors, since these peaks appear for both doped and undoped NP samples. These traces can affect the luminescence properties [54]. On the other hand, in the spectrum corresponding to the OxGC dried at 75 °C (green plot), a sharp band is identified at about 1260 cm⁻¹ together with a small band at 600 cm⁻¹ associated with Si-CH₃ groups from the silica precursor. The band at 1260 cm⁻¹ remains after the heat treatment (red plot), indicating the presence of Si-CH₃ groups. In both OxGCs spectra (green and red plots), a broad band between 1200 and 1000 cm⁻¹ is assigned to Si-O-Si bonds, with overlapping bands such as the 1040 cm⁻¹ and 1170 cm⁻¹ peaks associated with the transversal optical (TO) and longitudinal optical (LO) asymmetric stretching modes of Si-O-(Si), respectively, and possible Gd-O bonds (at 1114 cm⁻¹) overlapped with Si-O-Si vibrations, also identified in the 1.5Eu³⁺: NaGdF₄ NPs (blue plot). On the other hand, a small broad band is observed around 930 cm⁻¹, associated with Si-O(H) stretching vibration and/or non-bridging oxygen vibration. This band disappears after the heat treatment of OxGC, confirming the cross-linking of the SiO₂ network. A further band around 800 cm⁻¹ corresponds to the deformation vibration of

silicate tetrahedrons (O-Si-O) and Gd-O bonds. The vibration band appearing at 472 cm^{-1} is assigned to deformation vibrations of silicate tetrahedrons, ν_4 (O-Si-O), which becomes better defined after the heat treatment of OxGC (red plot). Finally, in both OxGCs spectra, the band around 400 cm^{-1} associated with crystalline tetrafluoride, also identified in the NP spectrum (blue line), is difficult to assign due to the proximity of the silicate tetrahedrons band and the limitation of the equipment [13].

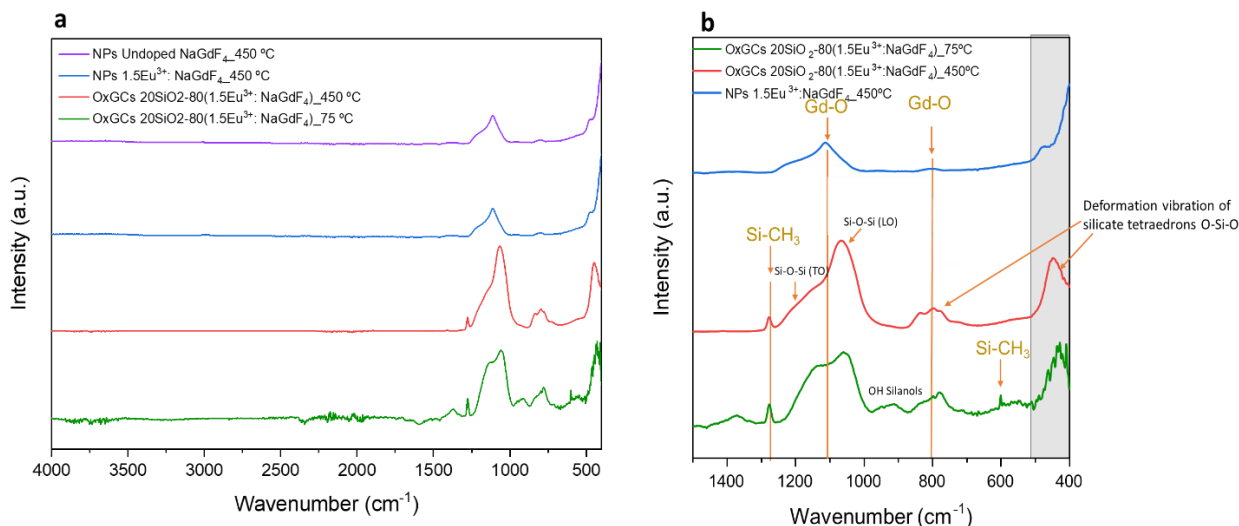


Figure 4. (a) FTIR spectra from 4000 cm^{-1} to 450 cm^{-1} of undoped NaGdF₄ NPs, 1.5Eu³⁺: NaGdF₄ NPs (violet and blue line, respectively) and OxGCs with the composition 80SiO₂-20(1.5Eu³⁺: NaGdF₄) dried overnight at 75 °C and heat-treated at 450 °C for 5 h (red and green line, respectively) and (b) FTIR spectra recorded from 1500 to 400 cm^{-1} of 1.5Eu³⁺: NaGdF₄ NPs and 80SiO₂-20(1.5Eu³⁺: NaGdF₄) OxGCs with the composition (blue, red and green line, respectively).

These results confirm the successful incorporation of the 1.5Eu³⁺: NaGdF₄ nanoparticles into the silica sol as their presence was evidenced both in the XRD pattern and FTIR spectra. However, the partial crystal transformation that takes place during the formation of the sol, from hexagonal to orthorhombic, should affect the optical properties of the OxGCs due to a reduction in the crystal symmetry. Nevertheless, molecular characteristics of the nanoparticles, such as the oxygen defect revealed in the FTIR spectra, suggest that the hexagonal nanoparticles that remain keep their properties throughout the sol formation.

3.3. Luminescence Properties of 1.5Eu³⁺: NaGdF₄ NPs

Figure 5a shows the excitation spectrum of the heat-treated 1.5Eu³⁺: NaGdF₄ NPs recorded by monitoring the $^5\text{D}_0 \rightarrow ^7\text{F}_2$ emission of Eu³⁺ at 615 nm. The spectrum shows a broad band centred around 245 nm attributed to the Eu³⁺-O₂-charge transfer band (CTB). The CTB reflects the accommodation of oxygen into a lattice of the NaGdF₄ NPs, which has already been reported for fluoride nanoparticles prepared via wet chemistry [38], and it is in concordance with the FTIR spectra shown in Section 3.2, where oxygen bonds have been identified. In addition to the CTB, the spectrum shows a peak at 272 nm attributed to the $^8\text{S}_{7/2} \rightarrow ^6\text{I}_J$ transition of Gd³⁺ and the $^7\text{F}_0 \rightarrow ^5\text{L}_6$ peak of Eu³⁺ at 395 nm. The presence of the Gd³⁺ peak in the excitation spectrum obtained by monitoring the Eu³⁺ luminescence confirms the Gd-Eu energy transfer. The other two small peaks at 423 and 501 nm are from the xenon lamp used for excitation.

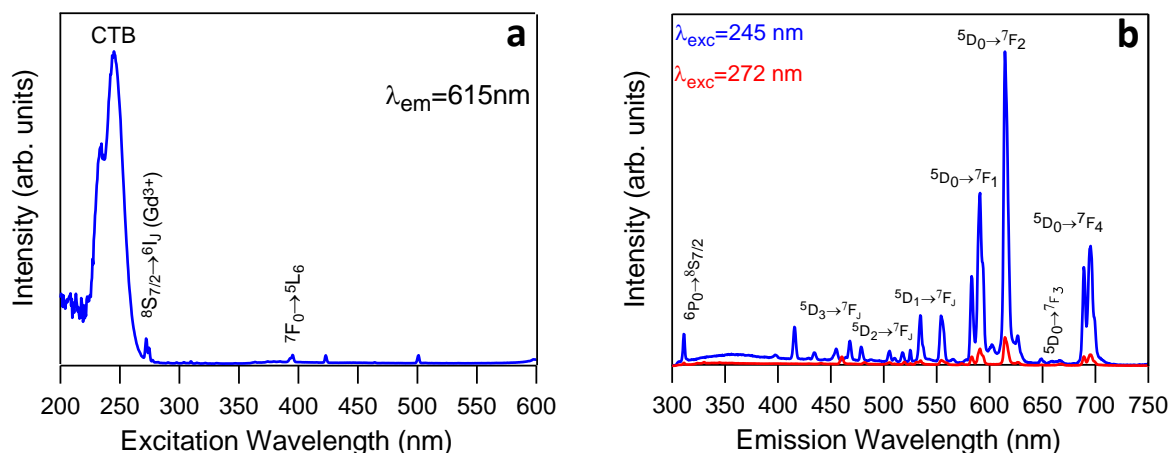


Figure 5. (a) Excitation spectrum of Eu^{3+} and Gd^{3+} ions from $1.5\text{Eu}^{3+}:\text{NaGdF}_4$ NPs heat-treated at 450°C for 5 h, collecting the luminescence at 615 nm. (b) Emission spectra of Eu^{3+} and Gd^{3+} ions from $1.5\text{Eu}^{3+}:\text{NaGdF}_4$ NPs heat-treated at 450°C for 5 h, excited at 245 nm (blue line) and 272 nm (red line).

The emission spectra of the $1.5\text{Eu}^{3+}:\text{NaGdF}_4$ NPs, shown in Figure 5b, were obtained under excitation at 245 nm (CTB) and 272 nm ($^8\text{S}_{7/2}\rightarrow^6\text{I}_1$) (Gd^{3+}), respectively. The spectra show the Gd^{3+} emission ($^6\text{P}_0\rightarrow^8\text{S}_{7/2}$) around 311 nm together with the Eu^{3+} emissions. The Gd^{3+} emission appears superimposed to a weak broad band centred at around 360 nm, likely associated with the $4f^65d-4f^7$ transition of Eu^{2+} . For both excitations, the main emissions correspond to the $^5\text{D}_0\rightarrow^7\text{F}_j$ transitions of Eu^{3+} . A small contribution of the $^5\text{D}_{1,2,3}\rightarrow^7\text{F}_j$ transition is also observed. The observed wavelength emissions, shown in Table 1, are similar to those published in the literature for other fluoride phases, such as GdF_3 or NaLaF_4 . Moreover, the emission spectrum obtained after excitation through the charge transfer band ($\lambda_{\text{exc}} = 245$ nm) is much higher in intensity than that obtained after Gd^{3+} excitation at 272 nm, in accordance with the most efficient energy transfer.

The most intense peak of the spectra corresponds to the electric dipole $^5\text{D}_0\rightarrow^7\text{F}_2$ transition, indicating that Eu^{3+} ions are in a non-centrosymmetric site; the intensity of this hypersensitive transition is strongly affected by the local field [55]. The asymmetry ratio, R , defined as the ratio of the $^5\text{D}_0\rightarrow^7\text{F}_2$ and $^5\text{D}_0\rightarrow^7\text{F}_1$ emission intensities, was calculated to describe this behaviour. The lower this value, the closer the local symmetry is to the one with an inversion centre [55]. The obtained value of 1.46 confirms the non-centrosymmetric site, which can be attributed to the substitution of a F^- ion by an O^{2-} ion in the coordination environment of an Eu^{3+} which lowers the site symmetry of the Eu^{3+} in the oxygen-free NaGdF_4 crystal [54].

In addition, the quantum yield calculated under excitation at $\lambda_{\text{exc}} = 270$ nm for the $1.5\text{Eu}^{3+}:\text{NaGdF}_4$ NPs gives a value of 43.1%. The quantum yield of Eu^{3+} -doped fluorides with Gd^{3+} ions has been calculated by many authors, most of them reporting a theoretical value of 200% due to the energy transfer between Gd^{3+} and Eu^{3+} with exciting Gd^{3+} [56–58]. The low emission efficiency after Gd^{3+} excitation, evidenced through the quantum yield value, could be due to the presence of oxygen impurities in the NaGdF_4 nanoparticles, as it is known that even a small amount of oxygen in the vicinity of Eu^{3+} ions can lead to a reduction in the photon emission [9].

The experimental decay curve from the $^5\text{D}_0$ level was obtained by exciting at 245 nm through the CTB and collecting the luminescence of the $^5\text{D}_0\rightarrow^7\text{F}_2$ transition at 615 nm. The decay curve, displayed in Figure 6, shows a rise time of 0.44 ms, due to the population of the $^5\text{D}_0$ level from higher energy levels, followed by a single exponential decay with a lifetime of 9.6 ms. This lifetime value is longer than some of those reported for hexagonal nanoparticles with the composition $\text{Eu}^{3+}:\text{NaYF}_4$ or $\text{Eu}^{3+}:\text{NaGdF}_4$ [59–61] and is similar to that found by Karbowski et al. for $\text{Eu}^{3+}:\text{NaGdF}_4$ nanocrystals [62].

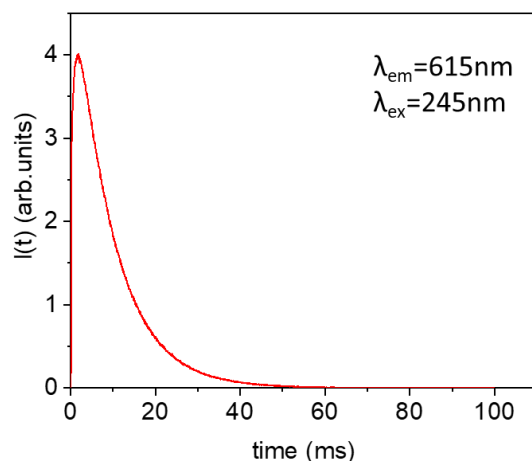


Figure 6. Experimental decay curve from 5D_0 level of Eu^{3+} in $1.5\text{Eu}^{3+}:\text{NaGdF}_4$ NPs heat-treated at 450°C for 5 h, taken under excitation at 245 nm and collecting the luminescence at 615 nm.

3.4. Luminescence Properties of $80\text{SiO}_2\text{-}20(1.5\text{Eu}^{3+}\text{NaGdF}_4)$ OxGCs

The luminescent properties of the OxGCs powders with the composition $80\text{SiO}_2\text{-}20(1.5\text{Eu}^{3+}\text{-}20\text{NaGdF}_4)$ heat-treated at 450°C for 5 h are presented in Figure 7a, which shows the emission spectrum recorded under excitation at 245 nm. The spectral features are similar to those obtained for $1.5\text{Eu}^{3+}:\text{NaGdF}_4$ NPs, with the peaks revealing the transition $^6P_0 \rightarrow ^8S_{7/2}$ of Gd^{3+} and the $^5D_0 \rightarrow ^7F_J$ transition from the Eu^{3+} ion. In addition to the nanoparticles study, the most intense peak was found to be corresponding to the $^5D_0 \rightarrow ^7F_2$ transition, in agreement with a non-centrosymmetric site for the Eu^{3+} ion. In this case, the calculated R-value is also 1.46, which is similar to that of the NPs. Furthermore, the wavelength of the emissions is the same as that detected for the nanoparticles reported in the previous section.

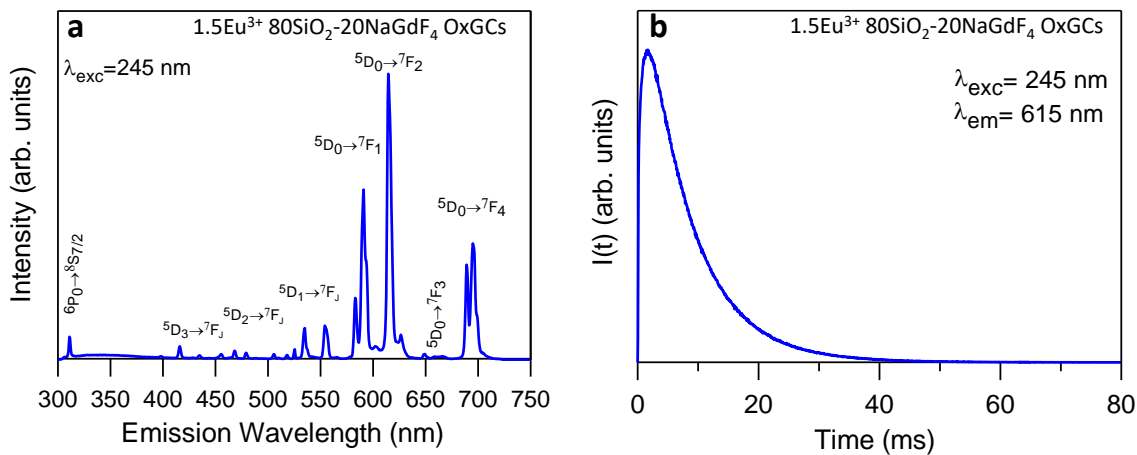


Figure 7. (a) Emission spectrum of Eu^{3+} and Gd^{3+} ions from OxGCs powders with the composition $80\text{SiO}_2\text{-}20(1.5\text{Eu}^{3+}:\text{NaGdF}_4)$ under excitation at 245 nm and (b) experimental decay curve from the 5D_0 level obtained by collecting the luminescence at 615 nm.

Figure 7b shows the luminescence decay curve from the 5D_0 level recorded while collecting the emission at 615 nm and exciting the CTB at 245 nm. The wavelength emissions are listed in Table 1. The lifetime value obtained was 7.9 ms, which was lower than the one obtained for the nanoparticles (9.6 ms). The decrease in the lifetime value could be due to the presence of the remaining organics in the silica matrix from the sol-gel precursor, as shown in the FTIR spectra of Section 3.2, where a peak of CH_3 from the MTES was identified. Moreover, the rising time was 0.4 ms, which was similar to that from the NPs.

Table 1. Emission wavelengths corresponding to the observed transitions of Gd³⁺ and Eu³⁺ in NPs and OxGCs.

Observed Transitions	Wavelength (Figures 5b and 7a)	NaGdF ₄ [63]	NaLaF ₄ [64,65]	EuF ₃ [66]	GdF ₃ [67]
⁶ P ₀ → ⁸ S _{7/2}	311 nm				
⁵ D ₃ → ⁷ F ₁	415.5 nm				
⁵ D ₃ → ⁷ F ₂	429 nm				
⁵ D ₃ → ⁷ F ₃	434.5 nm				
⁵ D ₃ → ⁷ F ₄	468 nm				
⁵ D ₂ → ⁷ F ₂	478.5 nm				
⁵ D ₂ → ⁷ F ₃	505.5				
⁵ D ₁ → ⁷ F ₀	525 nm				
⁵ D ₁ → ⁷ F ₁	534.5 nm				
⁵ D ₁ → ⁷ F ₂	554 nm				
⁵ D ₀ → ⁷ F ₁	583 nm, 591 nm	592 nm	592 nm	590 nm	591 nm
⁵ D ₀ → ⁷ F ₂	614.5 nm	613 nm	615 nm	612/617 nm	615 nm
⁵ D ₀ → ⁷ F ₃	649 nm	653 nm	650 nm		652 nm
⁵ D ₀ → ⁷ F ₄	689 nm, 695.5 nm	695 nm	695 nm		

As mentioned before, the optical properties of trivalent Eu are highly sensitive to the local environment. Since the ⁵D₀ state is non-degenerative under any symmetry, the structure of the ⁵D₀→⁷F_J emissions is only determined by the splitting of the terminal levels caused by the local crystal field. Moreover, as the ⁷F₀ level is also non-degenerative, site-selective excitation within the ⁷F₀→⁵D₀ absorption band can be performed using fluorescence line narrowing (FLN) spectroscopy, useful for distinguishing between different local environments around the Eu³⁺.

Time-resolved fluorescence line-narrowed (TRFLN) spectra of the ⁵D₀→⁷F₀₋₂ transitions of 80SiO₂-20(1.5Eu³⁺: NaGdF₄) powders heat-treated at 450 °C for 5 h were obtained at 9 K using different resonant excitation wavelengths throughout the ⁷F₀→⁵D₀ transition with a time delay of 10 μs. Depending on the excitation wavelength, the emission spectra present different characteristics, mainly related to the relative intensity and the level splitting of the transitions.

Figure 8 shows the low temperature (9 K) ⁵D₀→⁷F₀₋₂ emission spectra, obtained under excitation at 578.6 nm and 579 nm, both with a time delay of 10 μs after the laser pulse. These excitation wavelengths correspond to the highest emission intensities, with the spectrum obtained at 578.6 nm being more intense. Under excitation at 578.6 nm (Figure 8a), the ⁵D₀→⁷F₁ transition displays three stark components, which is in agreement with an Eu³⁺ occupying a site with orthorhombic symmetry, point group C_{2v}, or lower [68]. The spectrum obtained under 579 nm excitation (Figure 8b) shows two components for the ⁵D₀→⁷F₁ transition. The presence of two components for the splitting of the ⁷F₁ level and three for the ⁷F₂ level is compatible with trigonal site symmetry (C₃, C_{3v}) for Eu³⁺ ions. It is well known that the expected space group for β-NaGdF₄ is P $\bar{6}$ where Gd³⁺ occupy point symmetry C_{3h} sites [38]. In this point symmetry, the ⁵D₀→⁷F₀ transition is forbidden and the number of lines for the ⁵D₀→⁷F_{1,2} transitions are two and one, respectively [68]. However, the spectrum in Figure 8b shows the presence of the resonant ⁵D₀→⁷F₀ line as well as two and three components for the ⁵D₀→⁷F_{1,2} emissions, respectively. This implies that a breaking symmetry occurs produced by lattice distortions which may reduce the original C_{3h} symmetry to C₃ according to the branching rules of the 32 point groups [69]. The presence of two distinguishable sites for Eu³⁺ ions is, therefore, compatible with the observed hexagonal and orthorhombic phases detected in the XRD patterns of the OxGCs powders.

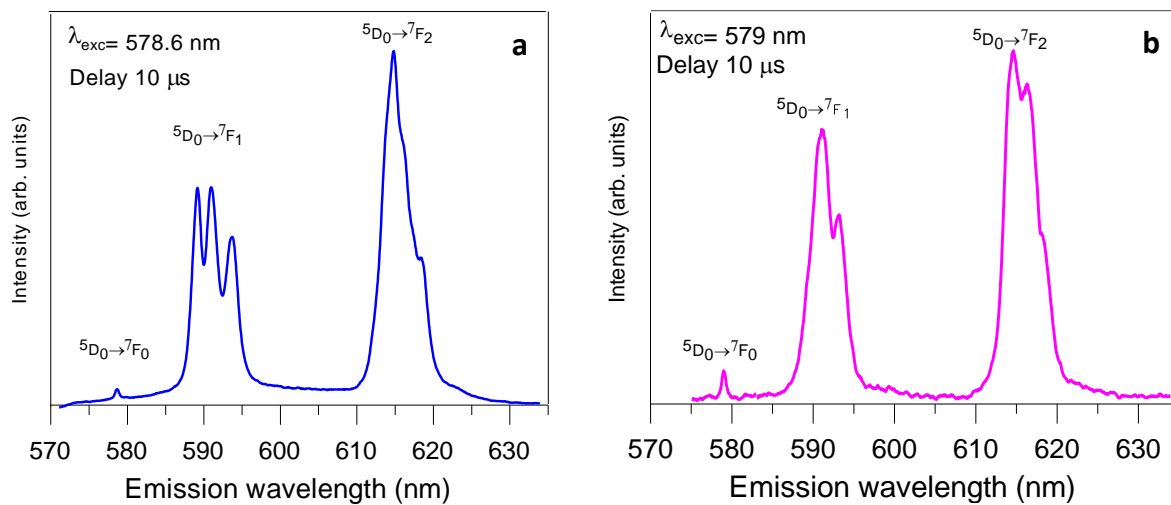


Figure 8. Time-resolved fluorescence line-narrowed emission spectra of the ${}^5D_0 \rightarrow {}^7F_{0,1,2}$ transitions of Eu^{3+} ions measured at 9 K at a time delay of 10 μs after the laser pulse under an excitation at (a) 578.6 nm and (b) 579 nm, respectively, for the $80\text{SiO}_2\text{-}20(1.5\text{Eu}^{3+}:\text{NaGdF}_4)$ powders heat-treated at 450 $^\circ\text{C}$ for 5 h.

4. Conclusions

Stable $1.5\text{Eu}^{3+}:\text{NaGdF}_4$ nanoparticle suspensions were successfully prepared via hydrothermal synthesis.

Nanoparticle synthesis is described as a process consisting of a first nucleation step, followed by a competition with the crystal growth.

XRD confirmed that hexagonal NaGdF_4 is the only present phase after sintering at 450 $^\circ\text{C}$ for 5 h.

FTIR spectra revealed that $1.5\text{Eu}^{3+}:\text{NaGdF}_4$ nanoparticles synthesised for 20 h present oxygen defects, probably forming Gd-O bonds.

In addition, nanoparticles present pores, likely due to the long synthesis process during which the crystal growth needs a much longer time than the nucleation step.

Although it is still possible to fit synthesis parameters to obtain better crystallised and defect-free hexagonal NaGdF_4 nanoparticles, these results are promising, opening a new route to prepare NaGdF_4 nanoparticle aqueous suspensions without any addition of organic dispersant.

It was confirmed that the acid media in which the OxGCs were prepared affects the stability of NaGdF_4 , generating a partial crystal transformation from hexagonal to orthorhombic.

Emission and excitation spectra together with the lifetimes of the 5D_0 state were measured for NPs and OxGCs with 1.5% Eu^{3+} . The excitation spectra showed the $\text{Eu}^{3+}\text{-O}^{2-}$ charge transfer band in accordance with the presence of oxygen in the lattice of the NPs. The emission spectra obtained by exciting the charge transfer band show similar features in both NPs and OxGCs, corresponding the higher emission intensity to the ${}^5D_0 \rightarrow {}^7F_2$ transition which indicates a non-centrosymmetric site for Eu^{3+} . The reduction in the lifetime value of the 5D_0 level from 9.6 ms in the NPs to 7.9 ms in OxGCs could be attributed to the presence of the remaining organics in the silica matrix. TRFLN spectra obtained under selective excitation in the ${}^7F_0 \rightarrow {}^5D_0$ absorption band at 9 K allow us to identify the existence of two distinguishable sites for Eu^{3+} ions in the OxGCs powders with C_{2v} and C_3 symmetries, which are compatible with the observed hexagonal and orthorhombic phases detected in the XRD diffraction patterns.

Author Contributions: Conceptualization, A.D. and Y.C.; Methodology, M.E.C., T.N.L.T. and R.B.; Formal analysis, M.E.C., T.N.L.T., A.C., R.B. and Y.C.; Investigation, M.E.C. and Y.C.; Data curation, M.E.C., A.D., J.F., R.B. and Y.C.; Writing—original draft, M.E.C. and Y.C.; Writing—review & editing, M.E.C., T.N.L.T., A.C., A.D., J.F., R.B. and Y.C.; Supervision, Y.C.; Funding acquisition, A.D. and R.B. All authors have read and agreed to the published version of the manuscript.

Funding: This project received funding from the European Union’s Horizon 2020 research and innovation program under grant agreement no. 739566. The authors acknowledge financial support from MICINN under projects PID2020-115419GB-C21-C22/AEI/10.13039/501100011033 and University of the Basque Country (Project GIU21/006).

Institutional Review Board Statement: Not applicable.

Informed Consent Statement: Not applicable.

Data Availability Statement: Data are available upon request.

Acknowledgments: The authors acknowledge financial support from MICINN under projects PID2020-115419GB-C21-C22/AEI /10.13039/501100011033 and from the University of the Basque Country (Project GIU21/006). This article is a part of the dissemination activities of the project Fun-Glass, which has received funding from the European Union’s Horizon 2020 research and innovation program under grant agreement No 739566.

Conflicts of Interest: The authors declare no conflict of interest.

References

1. Boulard, B.; Dieudonné, B.; Gao, Y.; Chiasera, A.; Ferrari, M. Up-conversion visible emission in rare-earth doped fluoride glass waveguides. *Opt. Eng.* **2014**, *53*, 071814. [[CrossRef](#)]
2. Cruz, M.E.; Castro, Y.; Durán, A. Glasses and Glass-Ceramics Prepared by Sol–Gel. *Ref. Modul. Mater. Sci. Mater. Eng.* **2020**, *2*, 695–708. [[CrossRef](#)]
3. Sharma, R.K.; Mudring, A.V.; Ghosh, P. Recent trends in binary and ternary rare-earth fluoride nanophosphors: How structural and physical properties influence optical behavior. *J. Lumin.* **2017**, *189*, 44–63. [[CrossRef](#)]
4. De Pablos-Martin, A.; Ferrari, M.; Pascual, M.J.; Righini, G.C. Glass-ceramics: A class of nanostructured materials for photonics. *Riv. Del Nuovo Cim.* **2015**, *38*, 311–369. [[CrossRef](#)]
5. Gorni, G.; Velázquez, J.J.; Mosa, J.; Balda, R.; Fernández, J.; Durán, A.; Castro, Y. Transparent glass-ceramics produced by Sol-Gel: A suitable alternative for photonic materials. *Materials* **2018**, *11*, 212. [[CrossRef](#)]
6. Sharma, R.K.; Ghosh, P. Lanthanide-Doped Luminescent Nanophosphors via Ionic Liquids. *Front. Chem.* **2021**, *9*, 715531. [[CrossRef](#)]
7. Fedorov, P.P.; Luginina, A.A.; Popov, A.I. Transparent oxyfluoride glass ceramics. *J. Fluor. Chem.* **2015**, *172*, 22–50. [[CrossRef](#)]
8. Alombert-Goget, G.; Armellini, C.; Berneschi, S.; Chiappini, A.; Chiasera, A.; Ferrari, M.; Guddala, S.; Moser, E.; Pelli, S.; Rao, D.N.; et al. Tb³⁺/Yb³⁺ co-activated Silica-Hafnia glass ceramic waveguides. *Opt. Mater.* **2010**, *33*, 227–230. [[CrossRef](#)]
9. Lezhnina, M.M.; Jüstel, T.; Kätker, H.; Wiechert, D.U.; Kynast, U.H. Efficient luminescence from rare-earth fluoride nanoparticles with optically functional shells. *Adv. Funct. Mater.* **2006**, *16*, 935–942. [[CrossRef](#)]
10. Biswas, K.; Sontakke, A.D.; Ghosh, J.; Annapurna, K. Enhanced blue emission from transparent oxyfluoride glass-ceramics containing Pr³⁺: BaF₂ nanocrystals. *J. Am. Ceram. Soc.* **2010**, *93*, 1010–1017. [[CrossRef](#)]
11. Dong, C.; Pichaandi, J.; Regier, T.; Van Veggel, F.C.J.M. Nonstatistical dopant distribution of Ln³⁺-doped NaGdF₄ nanoparticles. *J. Phys. Chem. C* **2011**, *115*, 15950–15958. [[CrossRef](#)]
12. Tissue, B.M. Synthesis and luminescence of lanthanide ions in nanoscale insulating hosts. *Chem. Mater.* **1998**, *10*, 2837–2845. [[CrossRef](#)]
13. Velázquez, J.J.; Mosa, J.; Gorni, G.; Balda, R.; Fernández, J.; Durán, A.; Castro, Y. Novel sol-gel SiO₂-NaGdF₄ transparent nano-glass-ceramics. *J. Non. Cryst. Solids* **2019**, *520*, 119447. [[CrossRef](#)]
14. Thoma, B.R.E.; Insley, H. The Sodium Fluoride-Lanthanide. *Inorg. Chem.* **1964**, *1005*, 1222–1229.
15. You, F.; Wang, Y.; Lin, J.; Tao, Y. Hydrothermal synthesis and luminescence properties of NaGdF₄:Eu. *J. Alloys Compd.* **2002**, *343*, 151–155. [[CrossRef](#)]
16. Sun, L.; Shi, S.; Geng, H.; Huang, Y.; Qiao, Y.; Song, J.; Yang, L.; Grimes, C.A.; Feng, X.; Cai, Q. NaGdF₄:Nd@NaGdF₄ Core-Shell Down-Conversion Nanoparticles as NIR-II Fluorescent Probes for Targeted Imaging of Bacteria. *ACS Appl. Nano Mater.* **2021**, *4*, 11231–11238. [[CrossRef](#)]
17. Chen, G.; Yang, C. Nanophotonics and Nanochemistry: Controlling the Excitation Dynamics for Frequency Up- and Down-Conversion in Lanthanide-Doped Nanoparticles. *Acc. Chem. Res.* **2013**, *46*, 1474–1486. [[CrossRef](#)]
18. Ramasamy, P.; Chandra, P.; Rhee, S.W.; Kim, J. Enhanced upconversion luminescence in NaGdF₄:Yb,Er nanocrystals by Fe³⁺ doping and their application in bioimaging. *Nanoscale* **2013**, *5*, 8711–8717. [[CrossRef](#)]

19. Xin, F.; Zhao, S.; Huang, L.; Deng, D.; Jia, G.; Wang, H.; Xu, S. Up-conversion luminescence of Er³⁺ - doped glass ceramics containing β -NaGdF₄ nanocrystals for silicon solar cells. *Mater. Lett.* **2012**, *78*, 75–77. [[CrossRef](#)]
20. Herrmann, A.; Tylkowski, M.; Bocker, C.; Rüssel, C. Cubic and hexagonal NaGdF₄ crystals precipitated from an aluminosilicate glass: Preparation and luminescence properties. *Chem. Mater.* **2013**, *25*, 2878–2884. [[CrossRef](#)]
21. Wei, Y.; Li, J.; Yang, J.; Chi, X.; Guo, H. Enhanced green upconversion in Tb³⁺-Yb³⁺ co-doped oxyfluoride glass ceramics containing LaF₃ nanocrystals. *J. Lumin.* **2013**, *137*, 70–72. [[CrossRef](#)]
22. Sarakovskis, A.; Kriekė, G. Upconversion luminescence in erbium doped transparent oxyfluoride glass ceramics containing hexagonal NaYF₄ nanocrystals. *J. Eur. Ceram. Soc.* **2015**, *35*, 3665–3671. [[CrossRef](#)]
23. Cao, J.; Chen, W.; Xu, D.; Hu, F.; Chen, L.P.; Guo, H. Wide-range thermometry based on green up-conversion of Yb³⁺/Er³⁺ co-doped KLu₂F₇ transparent bulk oxyfluoride glass ceramics. *J. Lumin.* **2018**, *194*, 219–224. [[CrossRef](#)]
24. Fiume, E.; Cao, S.P.O.; Na, M.; Migneco, C.; Vern, E. Comparison between Bioactive Sol-Gel and Melt-Derived Glasses/Glass-Ceramics Based on the Multicomponent SiO₂-P₂O₅-CaO-MgO-Na₂O-K₂O System. *Materials* **2020**, *13*, 540. [[CrossRef](#)] [[PubMed](#)]
25. Cruz, M.E.; Sedano, M.; Castro, Y.; Pascual, M.J.; Fernández, J.; Balda, R.; Durán, A. Rare-earth doped transparent oxyfluoride glass-ceramics: Processing is the key [Invited]. *Opt. Mater. Express* **2022**, *12*, 3493. [[CrossRef](#)]
26. Pierre, A.C. The Sol-Gel Chemistry of Oxides from Alkoxides. In *Introduction to Sol-Gel Processing*; Springer: Berlin/Heidelberg, Germany, 2020; ISBN 9783030381431.
27. Brinker, C.J.; Scherer, G.W. *Sol-Gel Science—The Physics and Chemistry of Sol-Gel Processing*; Academic Press, Inc.: San Diego, CA, USA, 1990; p. 462. [[CrossRef](#)]
28. Roy, R. Ceramics by the solution-sol-gel route. *Science* **1987**, *238*, 1664–1669. [[CrossRef](#)] [[PubMed](#)]
29. Hench, L.L.; West, J.K. The Sol-Gel Process. *Chem. Rev.* **1990**, *90*, 33–72. [[CrossRef](#)]
30. Cruz, M.E.; Castro, Y.; Durán, A. Transparent oxyfluoride glass-ceramics obtained by different sol-gel routes. *J. Sol-Gel Sci. Technol.* **2022**, *102*, 523–533. [[CrossRef](#)]
31. Gorni, G.; Velázquez, J.J.; Mosa, J.; Mather, G.C.; Serrano, A.; Vila, M.; Castro, G.R.; Bravo, D.; Balda, R.; Fernández, J.; et al. Transparent sol-gel oxyfluoride glass-ceramics with high crystalline fraction and study of re incorporation. *Nanomaterials* **2019**, *9*, 530. [[CrossRef](#)]
32. Cruz, M.E.; Durán, A.; Balda, R.; Fernández, J.; Mather, G.C.; Castro, Y. A new sol-gel route towards Nd³⁺ -doped SiO₂-LaF₃ glass-ceramics for photonic applications. *Mater. Adv.* **2020**, *1*, 3589–3596. [[CrossRef](#)]
33. Cruz, M.E.; Fernandez, J.; Durán, A.; Balda, R.; Castro, Y. Optically active nano-glass-ceramic coatings of Nd³⁺ doped-80SiO₂-20LaF₃ prepared by the pre-crystallized nanoparticles sol-gel route. *J. Non. Cryst. Solids* **2023**, *601*, 122050. [[CrossRef](#)]
34. Zhang, W.; Zang, Y.; Lu, Y.; Han, J.; Xiong, Q.; Xiong, J. Synthesis of Rare-Earth Nanomaterials Ag-Doped NaYF₄: Yb³⁺/Er³⁺ @ NaYF₄: Nd³⁺ + @ NaGdF₄ for In Vivo Imaging. *Nanomaterials* **2022**, *12*, 728. [[CrossRef](#)] [[PubMed](#)]
35. Ranasinghe, M.; Arifuzzaman, M.; Rajamanthiraj, A.C.; Willoughby, W.R.; Dickey, A.; McMillen, C.; Kolis, J.W.; Bolding, M.; Anker, J.N. X-ray excited luminescence spectroscopy and imaging with NaGdF₄:Eu and Tb. *RSC Adv.* **2021**, *11*, 31717–31726. [[CrossRef](#)]
36. Shao, Q.; Yang, C.; Chen, X.; Zhang, H.; Feng, G.; Zhou, S.; Zhou, S. Core-mediated synthesis, growth mechanism and near-infrared luminescence enhancement of α -NaGdF₄@ β -NaLuF₄:Nd³⁺ core-shell nanocrystals. *CrystEngComm* **2020**, *22*, 1359–1367. [[CrossRef](#)]
37. Rahman, P.; Green, M. The synthesis of rare earth fluoride based nanoparticles. *Nanoscale* **2009**, *1*, 214–224. [[CrossRef](#)] [[PubMed](#)]
38. Mech, A.; Karbowski, M.; Kępiński, L.; Bednarkiewicz, A.; Stręk, W. Structural and luminescent properties of nano-sized NaGdF₄:Eu³⁺ synthesised by wet-chemistry route. *J. Alloys Compd.* **2004**, *380*, 315–320. [[CrossRef](#)]
39. Karbowski, M.; Mech, A.; Bednarkiewicz, A.; Stręk, W. Structural and luminescent properties of nanostructured KGdF₄:Eu³⁺ synthesised by coprecipitation method. *J. Alloys Compd.* **2004**, *380*, 321–326. [[CrossRef](#)]
40. Sudheendra, L.; Das, G.K.; Li, C.; Stark, D.; Cena, J.; Cherry, S.; Kennedy, I.M. NaGdF₄:Eu³⁺ nanoparticles for enhanced X-ray excited optical imaging. *Chem. Mater.* **2014**, *26*, 1881–1888. [[CrossRef](#)] [[PubMed](#)]
41. Xu, D.K.; Yang, S.H.; Zhang, Y.L. Down-converted luminescence and energy transfer of α -KGd_{1-x}Eu_xF₄ nanophosphors with selective excitation. *J. Lumin.* **2013**, *143*, 298–303. [[CrossRef](#)]
42. Khan, L.U.; Khan, Z.U.; Rodrigues, R.V.; da Costa, L.S.; Gidlund, M.; Brito, H.F. Synthesis and characterization of tunable color upconversion luminescence β -NaGdF₄:Yb³⁺,Er³⁺ nanoparticles. *J. Mater. Sci. Mater. Electron.* **2019**, *30*, 16856–16863. [[CrossRef](#)]
43. Balda, R.; Fernández, J.; Adam, J. Time-resolved fluorescence-line narrowing and energy-transfer studies in a-doped fluorophosphate glass. *Phys. Rev. B-Condens. Matter Mater. Phys.* **1996**, *54*, 12076–12086. [[CrossRef](#)] [[PubMed](#)]
44. Chamuah, A.; Ojha, S.; Bhattacharya, K.; Ghosh, C.K.; Bhattacharya, S. AC conductivity and electrical relaxation of a promising Ag₂S-Ge-Te-Se chalcogenide glassy system. *J. Phys. Chem. Solids* **2022**, *166*, 110695. [[CrossRef](#)]
45. Da Silva, A.L.; de Oliveira, A.H.; Fernandes, M.L.S. Influence of preferred orientation of minerals in the mineralogical identification process by X-ray diffraction. In Proceedings of the INAC 2011: International Nuclear Atlantic Conference, Belo Horizonte, MG, Brazil, 24–25 October 2011; Volume 11.
46. He, F.; Yang, P.; Wang, D.; Niu, N.; Gai, S.; Li, X. Self-assembled β -NaGdF₄ microcrystals: Hydrothermal synthesis, morphology evolution, and luminescence properties. *Inorg. Chem.* **2011**, *50*, 4116–4124. [[CrossRef](#)] [[PubMed](#)]

47. Bogachev, N.A.; Betina, A.A.; Bulatova, T.S.; Nosov, V.G.; Kolesnik, S.S.; Tumkin, I.I.; Ryazantsev, M.N.; Skripkin, M.Y.; Mereshchenko, A.S. Lanthanide-Ion-Doping Effect on the Morphology and the Structure of NaYF₄:Ln³⁺ Nanoparticles. *Nanomaterials* **2022**, *12*, 2972. [[CrossRef](#)]
48. Wu, Y.; Li, C.; Yang, D.; Lin, J. Rare earth β-NaGdF₄ fluorides with multiform morphologies: Hydrothermal synthesis and luminescent properties. *J. Colloid Interface Sci.* **2011**, *354*, 429–436. [[CrossRef](#)] [[PubMed](#)]
49. Teng, X.; Liang, X.; Maksimuk, S.; Yang, H. Synthesis of porous platinum nanoparticles. *Small* **2006**, *2*, 249–253. [[CrossRef](#)]
50. Liu, J.; Yu, H.; Zhang, L.; Dong, H.; Liu, S.; Zhao, L. Controlling the final phase of multiphase KGdF₄ materials via chemical synthesis and structural phase transition. *J. Mater. Sci. Mater. Electron.* **2020**, *31*, 18096–18104. [[CrossRef](#)]
51. Cruz, M.E.; Li, J.; Gorni, G.; Durán, A.; Mather, G.C.; Balda, R.; Fernández, J.; Castro, Y. Nd³⁺-doped- SiO₂-KLaF₄ oxyfluoride glass-ceramics prepared by sol-gel. *J. Lumin.* **2021**, *235*, 118035. [[CrossRef](#)]
52. Vijayaprasath, G.; Murugan, R.; Hayakawa, Y.; Ravi, G. Optical and magnetic studies on Gd doped ZnO nanoparticles synthesized by co-precipitation method. *J. Lumin.* **2016**, *178*, 375–383. [[CrossRef](#)]
53. Passuello, T.; Pedroni, M.; Piccinelli, F.; Polizzi, S.; Marzola, P.; Tambalo, S.; Conti, G.; Benati, D.; Vetrone, F.; Bettinelli, M.; et al. PEG-capped, lanthanide doped GdF₃ nanoparticles: Luminescent and T2 contrast agents for optical MRI multimodal imaging. *Nanoscale* **2012**, *4*, 7682–7689. [[CrossRef](#)]
54. Ptacek, P.; Schäfer, H.; Kömpe, K.; Haase, M. Crystal phase control of luminescing NaGdF₄:Eu³⁺ nanocrystals. *Adv. Funct. Mater.* **2007**, *17*, 3843–3848. [[CrossRef](#)]
55. Reisfeld, R.; Zigansky, E.; Gaft, M. Europium probe for estimation of site symmetry in glass films, glasses and crystals. *Mol. Phys.* **2004**, *102*, 1319–1330. [[CrossRef](#)]
56. Ghosh, P.; Tang, S.; Mudring, A.V. Efficient quantum cutting in hexagonal NaGdF₄:Eu³⁺ nanorods. *J. Mater. Chem.* **2011**, *21*, 8640–8644. [[CrossRef](#)]
57. Wegh, R.; Donker, H.; Meijerink, A.; Lamminmäki, R.; Hölsä, J. Vacuum-ultraviolet spectroscopy and quantum cutting for Gd³⁺ in LYF₄. *Phys. Rev. B-Condens. Matter Mater. Phys.* **1997**, *56*, 13841–13848. [[CrossRef](#)]
58. Lepoutre, S.; Boyer, D.; Mahiou, R. Quantum cutting abilities of sol-gel derived LiGdF₄:Eu³⁺ powders. *J. Lumin.* **2008**, *128*, 635–641. [[CrossRef](#)]
59. Rabouw, F.T.; Prins, P.T.; Norris, D.J. Europium-Doped NaYF₄ Nanocrystals as Probes for the Electric and Magnetic Local Density of Optical States throughout the Visible Spectral Range. *Nano Lett.* **2016**, *16*, 7254–7260. [[CrossRef](#)]
60. Pathak, T.K.; Kumar, A.; Swart, H.C.; Kroon, R.E. Effect of annealing on structural and luminescence properties of Eu³⁺ doped NaYF₄ phosphor. *Phys. B Condens. Matter* **2018**, *535*, 132–137. [[CrossRef](#)]
61. Liu, Y.; Tu, D.; Zhu, H.; Li, R.; Luo, W.; Chen, X. A strategy to achieve efficient dual-mode luminescence of Eu³⁺ in Lanthanides doped multifunctional NaGdF₄ nanocrystals. *Adv. Mater.* **2010**, *22*, 3266–3271. [[CrossRef](#)] [[PubMed](#)]
62. Karbowiak, M.; Mech, A.; Bednarkiewicz, A.; Stręk, W.; Kępiński, L. Comparison of different NaGdF₄:Eu³⁺ synthesis routes and their influence on its structural and luminescent properties. *J. Phys. Chem. Solids* **2005**, *66*, 1008–1019. [[CrossRef](#)]
63. Zhang, W.; Shen, Y.; Liu, M.; Gao, P.; Pu, H.; Fan, L.; Jiang, R.; Liu, Z.; Shi, F.; Lu, H. Sub-10 nm Water-Dispersible β-NaGdF₄:X% Eu³⁺ Nanoparticles with Enhanced Biocompatibility for in Vivo X-ray Luminescence Computed Tomography. *ACS Appl. Mater. Interfaces* **2017**, *9*, 39985–39993. [[CrossRef](#)] [[PubMed](#)]
64. Tuomela, A.; Pankratov, V.; Sarakovskis, A.; Doke, G.; Grinberga, L.; Vielhauer, S.; Huttula, M. Oxygen influence on luminescence properties of rare-earth doped NaLaF₄. *J. Lumin.* **2016**, *179*, 16–20. [[CrossRef](#)]
65. Ladol, J.; Khajuria, H.; Khajuria, S.; Sheikh, H.N. Hydrothermal synthesis, characterization and luminescent properties of lanthanide-doped NaLaF₄ nanoparticles. *Bull. Mater. Sci.* **2016**, *39*, 943–952. [[CrossRef](#)]
66. Zhu, L.; Liu, X.; Meng, J.; Cao, X. Facile sonochemical synthesis of single-crystalline europium fluoride with novel nanostructure. *Cryst. Growth Des.* **2007**, *7*, 2505–2511. [[CrossRef](#)]
67. Kasturi, S.; Sivakumar, V.; Jeon, D.Y. Europium-activated rare earth fluoride (LnF₃:Eu³⁺–Ln = La, Gd) nanocrystals prepared by using ionic liquid/NH₄F as a fluorine source via hydrothermal synthesis. *Luminescence* **2016**, *31*, 1138–1145. [[CrossRef](#)]
68. Binnemans, K. Interpretation of europium(III) spectra. *Coord. Chem. Rev.* **2015**, *295*, 1–45. [[CrossRef](#)]
69. Butler, P.H. *Point Group Symmetry Application: Method and Tables*; in Plenum 5; Springer: Berlin/Heidelberg, Germany, 1981.

Disclaimer/Publisher's Note: The statements, opinions and data contained in all publications are solely those of the individual author(s) and contributor(s) and not of MDPI and/or the editor(s). MDPI and/or the editor(s) disclaim responsibility for any injury to people or property resulting from any ideas, methods, instructions or products referred to in the content.